Automated Corrected MAR Calculation for Characterisation of AE Signals

John MCCRORY*, Safaa Kh. AL-JUMAILI**, Matthew PEARSON*, Mark EATON*,
Karen HOLFORD*, Rhys PULLIN*
*Cardiff University, Cardiff, United Kingdom, UK, CF24 3AA
**University of Basrah, Basrah, Iraq
mccroryjp@cardiff.ac.uk

Abstract. Measured Amplitude Ratio (MAR) is a form of modal analysis for the classification of Acoustic Emission (AE) signals. MAR uses a comparison of the amplitudes of the first two primary lamb wave modes, symmetric (S_0) and asymmetric (A_0), to determine the orientation of the damage mechanisms in relation to the sensor. Previous researchers have demonstrated that some damage mechanisms, such as delamination in composite panels, inherently produce and out-of-plane movement and so are expected to generate signals with an MAR value below one. On the contrary, other mechanisms, such as matrix cracking, have been connected to in-plane movements and so generate signals with an MAR value above one. Typically, the technique can consume much of the users time as it involves scrutinising many waveforms individually in order to record the amplitudes of their lamb wave mode constituents. Furthermore, due to the nature of each lamb wave mode to attenuate at different rates, the MAR of a single source might appear to be different depending on source to sensor distance. This problem is amplified in larger structures, where differences in lamb wave mode attention have more distance over which to diverge. An automated MAR calculation method that corrects for the attenuation of each lamb wave mode separately is proposed and discussed. The developed technique successfully differentiated sources of matrix cracking and delamination in a composite panel subjected to buckling. Results were validated post-test using c-scanning, digital image correlation and visual inspection.

Introduction

The increasingly stringent regulations surrounding aircraft emissions, as well as the desire to reduce fuel consumption for the obvious cost benefits, have led to a dramatic increase in the use of composite materials in the civil aviation industry in recent years; from under 10% in the 1980's up to 53% in 2014 (percentages of total aircraft weight) [1]. Composite materials have been adopted to such a wide extent predominantly due to their superior strength-to-weight ratio when compared to conventional aerospace grade metals, though they also offer a number of additional benefits including greater corrosion and fatigue resistance.

It is widely known that aircraft are routinely inspected to assess their structural integrity; this is known as non-destructive testing (NDT) and is commonly attributed to being one of the key reasons for the success of the civil aviation industry. Thus, like all other aircraft components, the newer, composite components must also be subjected to NDT. However, despite their advantageous mechanical properties, composite materials are more difficult to inspect for damage than conventional metals and a number of traditional techniques, such as eddy current testing, do not

work at all. Of particular importance when monitoring composite components is the ability to detect the presence of delaminations; these are defined as the debonding of two or more plies in a laminate composite and can cause a dramatic reduction in the load bearing capacity of the structure [2]. Furthermore, since delaminations can be induced by a number of different loading scenarios its detection is paramount to the successful integration of composite materials into aircraft structures.

One damage detection method that might provide a solution is acoustic emission (AE); which is defined as the transient elastic energy released when a material undergoes changes at the atomic level, such as plastic deformation or cracking. AE, which has already seen use on a number of composite structures such as pressure vessels, is unlike other detection methods in that it has the benefit of being a passive technique and so lends itself to be used as part of an automated Structural Health Monitoring (SHM) system. Furthermore, AE offers the ability to not only detect damage but also locate and potentially characterise the source mechanism; this would prove useful for the inspection of composite materials since their complex structures means that they can be subject to numerous damage mechanisms and knowledge of which damage mechanism is taking place would allow the end user of an SHM system to assess the level of danger presented by the damage. This study investigates one such AE characterisation technique known as measured amplitude ratio (MAR) and attempts to improve upon the known existing method in order to increase the accuracy of the characterisation process. A buckling test involving a carbon fibre panel is used to demonstrate the adjusted technique.

1. Measured Amplitude Ratio

It is well known that AE waves traveling in flat plates propagate as Lamb waves [3]. The movement of the plate's two surfaces couple and guide the wave, known as the wave-guide effect; typically the wave must be traveling in the plate for a distance approximately ten times the plate thickness for this coupled motion to be established. Once Lamb wave motion has been established, the AE wave travels via two distinctive propagation modes; longitudinal waves, in the plane of the surface, and transverse waves, perpendicular to the plane of the surface, Figure 1. It is possible for multiple order longitudinal and transverse mode waves to propagate, however this is only apparent for large plate thicknesses and it is only the zero-order modes that exist across all frequencies. The zero-order longitudinal and transverse waves are often referred to as extensional and flexural waves or S_o and A_o waves respectively.

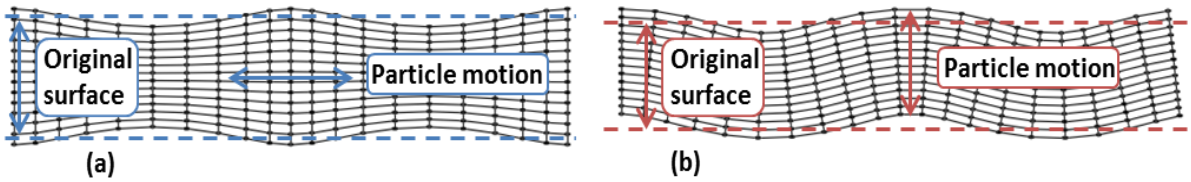

Figure 1: a) Longitudinal, S_o Lamb wave mode b) Transverse, A_o Lamb wave mode [4]

Due to their nature, some damage mechanisms have a tendency to excite more of one Lamb wave mode than another and so studies have identified the possibility of using a 'modal analysis' to classify events [5]; using the relationship between the S_o and A_o wave modes to distinguish between damage mechanisms occurring in plate like structures. Using this technique, previous studies have found that damage which causes an out-of-plane movement of the structure, for instance delamination, will excite more energy in the flexural, A_o mode and damage of an in-plane nature, such as matrix cracking, will excite more energy in the extensional, S_o mode [6, 7], Figure 2. Thus, calculating the ratio of the S_o to A_o mode amplitudes will reveal whether the signals are S_o mode dominant (MAR>1) or A_o mode dominant (MAR<1) and hence suggests the nature of the damage present.

$$MAR = \frac{So\ amplitude}{Ao\ amplitude}$$

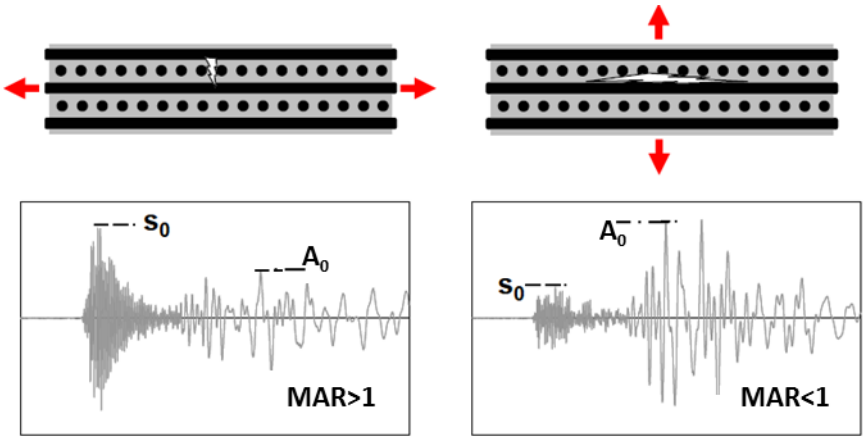

Figure 2: Example of in-place and out-of-plane sources [8]

2. Corrected MAR

Using MAR, previous studies have managed to successfully classify signals by the orientation of their source mechanism in small composite specimens [8]. However, it is understood that the attenuation of the S_o and A_o wave modes are dissimilar in composite materials [9, 10] which is detrimental to the classification of damage using MAR on large-scale structures since the MAR will vary depending on the source to sensor propagation path. Furthermore, previous studies have required the user to manually calculate the MAR of signals, which is very time consuming and subject to the user's interpretation. To overcome these problems, a novel form of automated MAR calculation is proposed which corrects for the attenuation of both wave modes separately before making the amplitude ratio calculation. Each step of the process is outlined below;

1. The traveling frequencies of the S_o and A_o wave modes as well their attenuation behaviours are established empirically
2. The predicted locations of detected signals are compared to the known locations of the recording sensors to establish their propagation paths
3. The S_o and A_o amplitudes of located signals are separated from one another using the time of flight information and band pass filters
4. The S_o and A_o amplitudes are corrected based on their predicted path and attenuation behaviour
5. The MAR of each recorded signal is calculated after correction

2.1 Propagation Study Investigation

The automated, corrected MAR analysis is demonstrated here using the data collected in a propagation study. To this end, a propagation study of an eight ply layup of Umeco MTM®44-1 unidirectional carbon fibre, with the configuration $(0,90)_{4s}$, was performed using four wideband, MISTRASS Group Limited (MGL) WD sensors (100-1000kHz). The sensors were placed 70mm apart, in a line along the 0^o material direction and held in place between magnets positioned on both surfaces of the panel; multipurpose, brown grease was used as the acoustic couplant. The sensors were connected to MGL pre-amplifiers, set to a gain of 40dB and with a frequency range of 20-1200kHz, and AE data was recorded using a MGL PCI2 acquisition system. Ten Hsu-Nielsen (H-N) sources [11] were generated at a distance of 10mm behind the first sensor and the resultant signals were recorded for all four sensors. This process was repeated at 10^o intervals up to 90^o. The five steps of the MAR correction process outlined above are demonstrated with the data collected from this attenuation study.

1. The velocities of both wave modes, as well as examples of their attenuation behaviour are shown in Figure 3. The traveling frequencies of each wave mode in this material were obtained using a wavelet transform; there were found to be 150kHz-500kHz and 10kHz-150kHz for the S_o and A_o modes respectively.

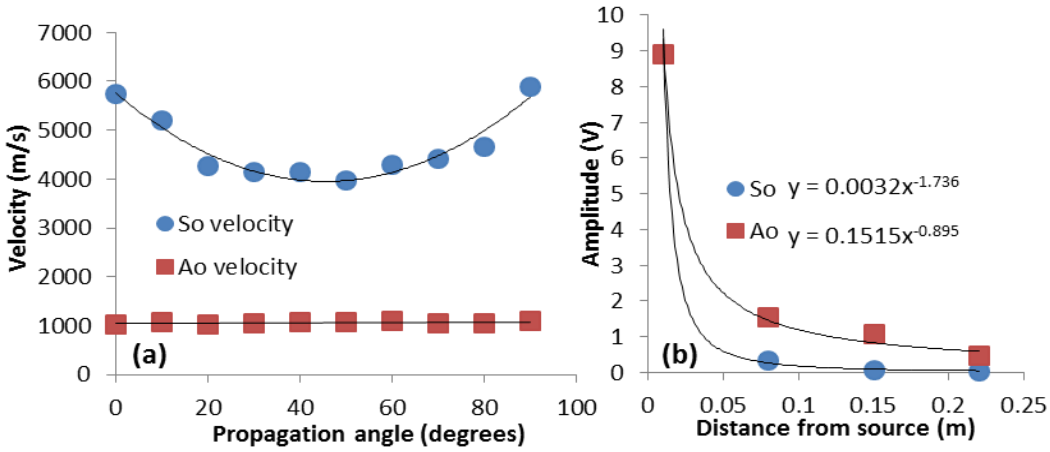

Figure 3: Propagation study results (a) velocity (b) attenuation for 50^{o}

2. For the purposes of this example a signal recorded by channel 3, when the sensors were aligned at 0^{o}, will be investigated. Therefore the propagation path in this example is 150mm at 0^{o}.
3. Knowledge of the pre-trigger length, sampling frequency, propagation path and velocities allow the S_o and A_o modes to be crudely isolated before the application of the band pass filters which act to further isolate each wave mode for investigation, Figure 4.

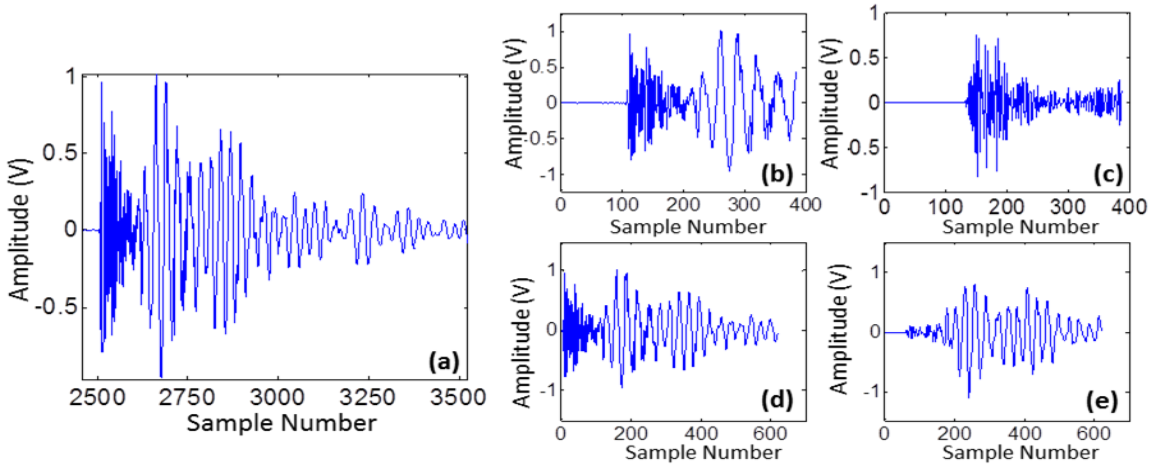

Figure 4: (a) Original signal (b) S_o mode sample extracted from original signal using time of flight (c) S_o mode calculated from sample using filter (d) A_o mode sample extracted from original signal using time of flight (e) A_o mode calculated from sample using filter

4. The amplitude correction process comprises of comparing the maximum amplitude of a wave mode sample to the amplitude of that mode's attenuation curve for the same propagation distance. The ratio of the two values is used to correct the equation for the attenuation curve and this new equation for the attenuation can be used to obtain the amplitude of that wave mode at any propagation distance. Figure 5 gives a graphical representation of this process for the correction of the S_o wave mode.
5. Using this corrected attenuation equation, the amplitudes of the S_o and A_o modes after 80mm of propagation were predicted and used to work out the predicted MAR at this distance; 0.794. Visual inspection of the signal recorded at channel 2, positioned 80mm from the H-N source reveals the actual MAR value of the signal after 80mm of propagation to be 0.74.

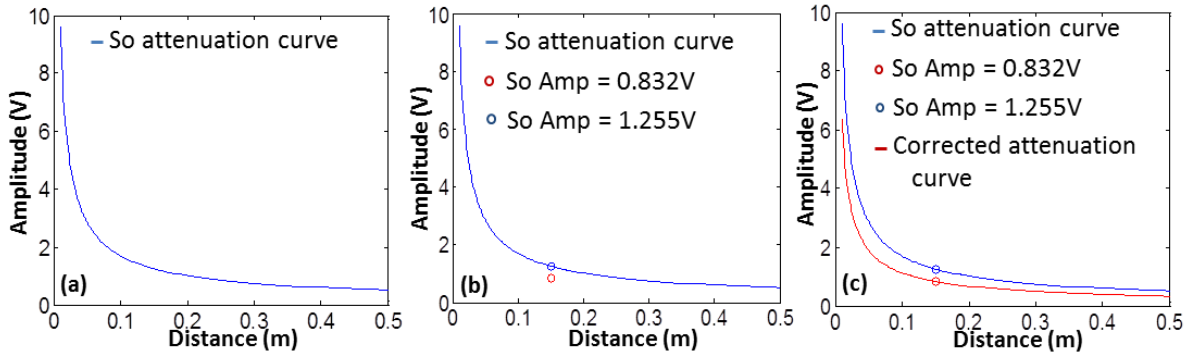

Figure 5: (a) Attenuation curve of S_o mode along 0^o (b) Amplitude of signal and attenuation curve, at the same distance, are compared (c) Corrected attenuation curve for this signal calculated

3. Buckling Test

A 403x376mm carbon fibre panel, cut from the same material as used in the propagation study, was subjected to a buckling test using the rig seen in Figure 2. The base and the left and right edges are prevented from moving in-plane whereas the top edge is free to move vertically downwards, thus allowing the plate to be compressed by applying a force to the top edge. Roller supports along the horizontal edges and sprung knife edges along the vertical sides provide simply supported boundary conditions on all four edges.

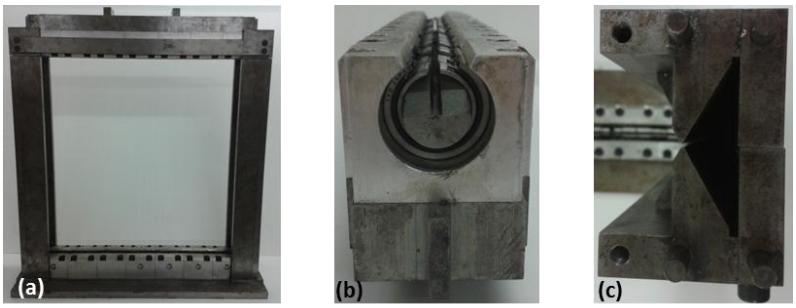

Figure 6: (a) Buckling test rig (b) Horizontal roller supports (c) Vertical knife edge supports

The specimen was ultrasonically c-scanned to ensure no damage had occurred during the cutting process after which a speckle pattern was applied to one side, using spray paint, to allow digital imaging correlation (DIC) monitoring; an optical technique that provides full-field displacement measurements of a structure [12]. Three MGL WD sensors (100-1000kHz) and five MGL Nano-30 sensors (125-750kHz) were chosen to be used in the experiment and the eight sensors were adhered to the surface in the positions shown in Figure 3 (a) using Loctite® 595, a multi-purpose clear silicone sealer, which also acted as the acoustic couplant between the panel and the sensors. The sensors were connected to MGL pre-amplifiers, set to a gain of 40dB and with a frequency range of 20-1200kHz and subsequently to an MGL PCI2 acquisition system.

Once prepared, the specimen was mounted into the rig and loaded in compression at a constant rate of 0.24 mm/min until failure occurred. AE data was recorded during this time and DIC images were captured manually approximately once every 1kN of increased loading.

3.1 Buckling Test Results

The specimen was removed from the test rig after failure occurred and visually inspected for damage; a region of delamination in the upper left corner of the panel was discovered. An ultrasonic c-scanned was then conducted to further assess the induced damage, Figure 3 (b), which revealed a

large area of high attenuation in the top left corner, due to the delamination damage there; the four additional spots of high attenuation observed near the panel centre are caused by the panel supports in the c-scan tank.

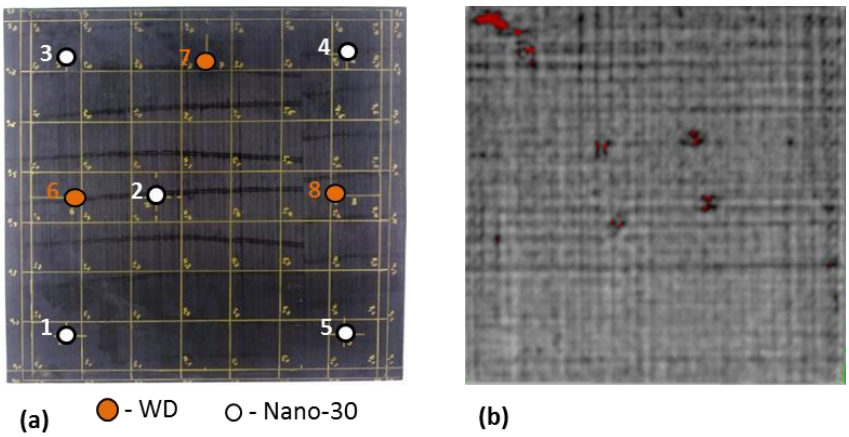

Figure 7: (a) Delta-T mapping grid and sensor positions (b) C-scanned image after buckling

Using the results of the DIC analysis to accurately determine the deflection of the panel, the onset of buckling was revealed to be 5kN. During post-buckling, the panel deformed with a constant stiffness until approximately 26kN at which point the stiffness dropped which is likely due to the onset of significant levels of damage within the panel. Final material failure occurred at 44.61kN.

3.2 Corrected MAR characterisation of AE signals

Since the corrected MAR characterisation process requires the propagation path to be known only located signals were analysed. Signal locations were obtained using delta-T mapping, a location algorithm developed at Cardiff University, explained in detail by Baxter [13], which can provide increased accuracy over the conventional time-of-arrival (TOA) technique [13, 14]. Furthermore, because they offer a more wideband response, only signals recorded from the three WD sensors were analysed.

To distinguish between in-plane and out-of-plane sources the results of the corrected MAR analysis were analysed in terms of two groups, MAR>1 and MAR<1 respectively. Once the data was divided in this manner the cumulative number of hits and cumulative energy of each MAR group was plotted, to show the evolution of their activity over the course of the test, alongside the load trace, Figure 4; the drop in the load near the beginning of the test is due to the specimen settling into the test rig supports.

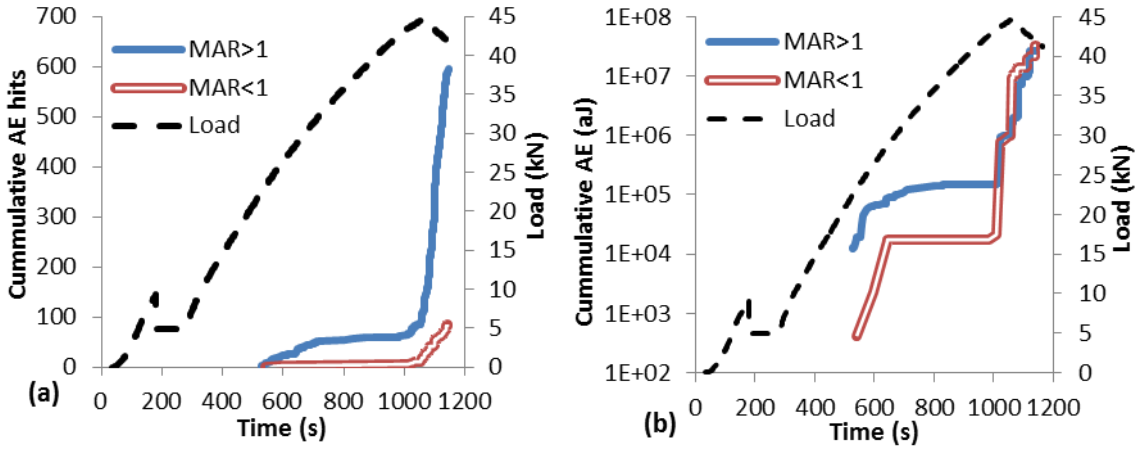

Figure 8: (a) cumulative hits with load for MAR>1 and MAR<1 signals (b) Cumulate AE energy with load for MAR>1 and MAR<1 signals classes

The curves of cumulative AE hits in Figure 4 (a) show that signals with an MAR>1 have an earlier onset and higher overall level of activity than signals with an MAR<1. There are two main periods during which MAR>1 signals are most active; firstly from approximately 550s to 700s and secondly

from approximately 920s until final failure. During the initial period of high activity of MAR>1 signals, at 580s, there is a significant jump in the cumulative recorded energy, Figure 4 (b); this corresponds to the point at which the DIC analysis identified the panel's stiffness to change. MAR<1 signals only begin to appear in abundance during the later stages of loading, shortly before and during the final failure of the material. It can also be seen in Figure 4 that, despite the fact that the total number of MAR<1 signals is approximately six times fewer than MAR>1 signals, the total energy contained within MAR<1 signals closely matches that of the MAR>1 signals meaning that, on average, signals with an MAR<1 contain more energy than signals with an MAR>1. Based on the data from these plots, the test was divided into 4 time segments as follows:

- Segment 1 from 0s to 580s (from the beginning, to the appearance of the first located events);
- Segment 2 from 580 s to 1000 s (up to the beginning of the second MAR>1 high-activity phase);
- Segment 3 from 1000 s to 1060 s (the onset of the MAR<1 high activity phase and peak load);
- Segment 4 from 1060 s to the end of the test and final material failure;

Combining the classification of signals with the delta-T mapping location results allows the hits belonging to each class to be plotted spatially; this was done for each time segment in order to show the evolution of classified signals spatially over time, Figure 5. It can be seen that the first located signals originate from the bottom-left corner of the panel and predominantly have a MAR>1. As the test progresses the activity of MAR>1 signals increases though only two more MAR<1 signals appear, on the left side the panel. After 1000s most activity is observed in the top-left corner with a large number of both MAR<1 and MAR>1 signals occurring until final failure. By the end of the test, large clusters of MAR>1 signals can be seen to have originated from the bottom-left, centre and top-left of the panel whereas the vast majority of MAR<1 signals appear to originate from the top-left corner and centre of the panel.

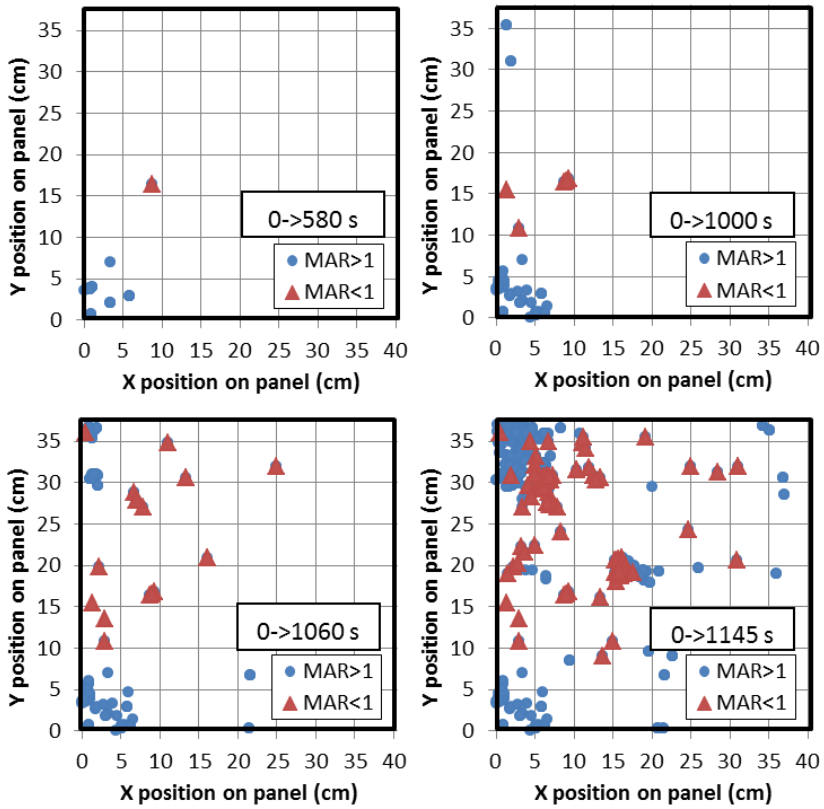

Figure 5: Historical distribution of UWC class 1 and class 2 signals during test

It is believed that a number of signals originating from the corners were mis-located as originating from the centre of the panel. Similar behaviour has been observed before [10]and it is believed to be in error here since the centre of the panel experiences the lowest curvature and, is

least likely to experience damage and emit AE. For this reason, signals located as originating from the centre of the panel will no longer be considered.

3.3 Corrected MAR Characterisation Discussion

The presence of both MAR>1 and MAR<1 signals suggests that there are at least two distinct, separate sources of AE signals arising in the panel during the buckling loading regime.

The C-scan inspection revealed an area of delamination at the top left corner of the panel, a common failure mode for CFRP subject to bending loads. This agrees with the result of the MAR analysis since MAR<1 signals, indicative of delamination [6, 7], are predominantly located in the top-left corner of the panel. Furthermore, since delamination typically occurs during the final failure of composite materials it is only likely to have a greater present in the final stages of testing, which corresponds to the activity seen from MAR<1 signals.

It is likely that MAR>1 signals arise from in-plane matrix damage since matrix cracking is commonly the first damage mechanisms to occur in CFRPs under quasistatic loading conditions [7, 9, 15] and the MAR>1 class signals are the first to appear in abundance during the test. This class has a large amount of activity around 600 s (26kN) where the stiffness of the specimen was observed to change and this reduction in stiffness could be attributed to the onset of significant matrix damage in the material. The second large jump in activity of MAR>1 signals, during final material failure, is likely due to the high curvature in the top-left of the panel, which occurs as a result of buckling and the specific restraints of the test rig, causing large enough strains for matrix cracking to take place. The build-up of this matrix damage progressively reduced the structural integrity of the corner until delamination occurred, thus causing the matrix structure to bear more of the load and crack further which leads to more delamination; hence the large increase in activity from both MAR<1 and MAR>1 signal during final failure. In this test, the MAR>1 signals are unlikely to be attributed to fibre failure, another conventionally in-plane source, as it is believed that the large bending in the corners caused a tearing motion leading delamination to occur before the fibres could fail.

4. Conclusion

The corrected MAR analysis was able to successfully distinguish between in-plane and out-of-plane signals arising in a carbon fibre panel subject to buckling whish lead to the characterisation of the damage occurring within the panel. Of notable relevance was the approaches ability to detect delaminaion as this is particularly detrimental to composite materials. This is the first time that this specific corrective-MAR approach has been used and the ease of interpretation of the results greatly assisted the characterisation process; signals identified as having an MAR>1 were attributed to matrix cracking, whereas signals with an MAR<1 were attributed to delamination.

The delta-T mapping location proved to be a powerful tool when used in conjunction with the characterisation technique by providing accurate location information for each event. This allowed the classified signals to be plotted spatially, providing more information about the classes and thus increased the accuracy with which they can be attributed to specific damage mechanisms.

The ability to classify signals in situ using a technique such as this would improve the capabilities of an SHM system, by informing the end user of the types of damage present in a structure, though more research must be done to make these techniques more robust and autonomous and, hence, less dependent on the interpretation of the user.

References

1. Society, R.A., *The Use of Composites in Aerospace: Past, Present and Future Challenges*, 2012.
2. Sridharan, S., *Delamination Behaviour of Composites*. 2008.

3. Center, N.R. *Modes of Sound Wave Propagation*. 11-07-2013]; Available from: http://www.ndt-ed.org/EducationResources/CommunityCollege/Ultrasonics/Physics/modepropagation.htm.
4. Seismic, P. *Multichannel Approach (MASW)*. 23-08-2013]; Available from: http://www.masw.com/History-MASW.html.
5. Surgeon, M. and M. Wevers, *Modal analysis of acoustic emission signals from CFRP laminates.* NDT and E International, 1999. **32**(6): p. 311-322.
6. Gorman, M.R. and S.M. Ziola, *Plate waves produced by transverse matrix cracking.* Ultrasonics, 1991. **29**(3): p. 245-251.
7. Dzenis, Y.A. and J. Qian, *Analysis of microdamage evolution histories in composites.* International Journal of Solids and Structures, 2001. **38**(10–13): p. 1831-1854.
8. Eaton, M., et al., *Characterisation of damage in composite structures using acoustic emission.* Journal of Physics: Conference Series, 2011. **305**(1).
9. Sause, M.G.R., et al., *Quantification of failure mechanisms in mode-I loading of fiber reinforced plastics utilizing acoustic emission analysis.* Composites Science and Technology, 2012. **72**(2): p. 167-174.
10. Eaton, M., *Acoustic Emission (AE) Monitoring of Buckling and Failure in Carbon Fibre Composite Structures*, in *Cardiff School of Engineering*2007, Cardiff University.
11. ASTM, *A standard guide for determining the reproducability of acoustic emission sensor responce*, 1994, American society for testing and materials.
12. Dynamics, D. *Measurement Principles of DIC*. 30-03-2013]; Available from: http://www.dantecdynamics.com/measurement-principles-of-dic.
13. Baxter, M.G., et al., *Delta T source location for acoustic emission.* Mechanical Systems and Signal Processing, 2007. **21**(3): p. 1512-1520.
14. Eaton, M.J., R. Pullin, and K.M. Holford, *Acoustic emission source location in composite materials using Delta T Mapping.* Composites Part A: Applied Science and Manufacturing, 2012. **43**(6): p. 856-863.
15. de Oliveira, R. and A.T. Marques, *Health monitoring of FRP using acoustic emission and artificial neural networks.* Computers and Structures, 2008. **86**(3-5): p. 367-373.